Redox Biology 57 (2022) 102488

Contents lists available at ScienceDirect

Redox Biology

journal homepage: www.elsevier.com/locate/redox

A versatile multiplexed assay to quantify intracellular ROS and cell viability in 3D on-a-chip models

Camilla Soragni [a,b,*], Gwenaëlle Rabussier [a,b], Henriëtte L. Lanz [a], Kristin M. Bircsak [a], Leon J. de Windt [b], Sebastiaan J. Trietsch [a], Colin E. Murdoch [c], Chee Ping Ng [a]

[a] MIMETAS BV, Leiden, the Netherlands
[b] Department of Cardiology, Maastricht University, Maastricht, the Netherlands
[c] Systems Medicine, School of Medicine, University of Dundee, Dundee, Scotland, UK

ARTICLE INFO

Keywords:
ROS
Cell viability
Multiplex assay
Organ-on-a-chip
Antioxidant
Oxidative stress
Angiogenesis

ABSTRACT

Reactive oxygen species (ROS) have different properties and biological functions. They contribute to cell signaling and, in excessive amounts, to oxidative stress (OS). Although ROS is pivotal in a wide number of physiological systems and pathophysiological processes, direct quantification *in vivo* is quite challenging and mainly limited to *in vitro* studies. Even though advanced *in vitro* cell culture techniques, like on-a-chip culture, have overcome the lack of crucial *in vivo*-like physiological aspects in 2D culture, the majority of *in* vitro ROS quantification studies are generally performed in 2D. Here we report the development, application, and validation of a multiplexed assay to quantify ROS and cell viability in organ-on-a-chip models. The assay utilizes three dyes to stain live cells for ROS, dead cells, and DNA. Confocal images were analyzed to quantify ROS probes and determine the number of nuclei and dead cells. We found that, in contrast to what has been reported with 2D cell culture, on-a-chip models are more prone to scavenge ROS rather than accumulate them. The assay is sensitive enough to distinguish between different phenotypes of endothelial cells (ECs) based on the level of OS to detect higher level in tumor than normal cells. Our results indicate that the use of physiologically relevant models and this assay could help unravelling the mechanisms behind OS and ROS accumulation. A further step could be taken in data analysis by implementing AI in the pipeline to also analyze images for morphological changes to have an even broader view of OS mechanism.

1. Introduction

Reactive Oxygen Species (ROS) are charged, uncharged or free radical oxidants mainly produced by oxidative metabolism [1]. ROS are involved in physiological [2] and pathological processes [3,4]. At low concentrations they act as signaling molecules [3,5–7], through oxidative post-translational modifications [8] they regulate cell proliferation, hypoxic environment adaptation [9] and cell shape [10]; they play a role in vascular tone [11] and angiogenesis regulation [12,13]. At high levels, ROS are harmful molecules which oxidize macromolecules and provoke structural cell damage which can lead to cell apoptosis [8]. This condition is called oxidative stress (OS) and is characterized by an increase in oxidants together with a depletion of antioxidant responses [14]. Intracellular ROS accumulation can contribute to endothelial dysfunction [15] and ischemic neo-vascularization [16]; it is implicated in atherosclerosis [17], endothelial mesenchymal transition [18], aging [19], hypertension [20], and cancer [13]. In angiogenesis, higher ROS levels are expected compared to quiescent endothelial cells (ECs) but lower compared to pathological angiogenesis as in cancer. In cancer it is known that the cause of increase in ROS is the uncontrolled angiogenesis and inflammatory state typical of this condition [13], while for other processes [21] such neurodegenerative diseases [22] the role played by OS is still not completely understood.

Quantification of ROS is a pivotal tool to understand the role of OS and ROS in pathological and physiological processes. Unfortunately, ROS quantification is quite challenging, mainly due to their highly reactive nature, short half-life, and localization in discrete sub-cellular compartments which limit their direct quantification generally to *in vitro* studies [5,23,24].

To overcome the limitation to directly quantify ROS *in vivo,* the use of physiologically relevant *in vitro* models is necessary. Advanced *in vitro* cell culture techniques, like 3D cell culture [25–27] or organ-on-a-chip,

* Corresponding author. MIMETAS BV, Leiden, the Netherlands.
E-mail address: c.soragni@maastrichtuniversity.nl (C. Soragni).

https://doi.org/10.1016/j.redox.2022.102488
Received 13 September 2022; Accepted 22 September 2022
Available online 29 September 2022

which include perfusion, extracellular matrix interactions, and a 3D structure, better mimic the complexity and physiology typical of the *in vivo* situation compared to traditional 2D cell culture [28]. While effects of ROS accumulation have been already studied in on-a-chip models to investigate the effect of ROS on barrier integrity in a blood-retinal model [29] or on cell viability in B lymphocyte [30], quantification of ROS has been realized only in 2D cell cultures where ROS content is often measured to study the effect of oxidant or antioxidants [31–36] in parallel with cell viability [37].

Here we report the development, validation and application of a scalable multiplexed versatile live-cell and image-based assay to quantify ROS accumulation or depletion together with cell viability in 3D organ-on-a-chip *in vitro* models. The ROS-viability assay utilized dihydrorhodamine 123 (DHR123), Hoechst and propidium iodide (PI) to stain for intracellular ROS, DNA and dead cells, respectively. Fluorescence intensity of ROS, normalized against cell count, and cell viability were quantified from the images acquired with a high-content (HC) fluorescence microscopy. We utilized a vasculature-on-a-chip model [38] to optimize exposure time and concentration of control to enhance ROS content with *tert*-butyl hydroperoxide (TBHP), we used the assay to quantify TBHP EC_{50} in the accumulation mode and gallic acid, tocopherol, resveratrol and curcumin to test the assay in depletion mode and to quantify the IC_{50} of these antioxidants. To validate the assay we tested standard media, TBHP, with and without curcumin and 0.1% of DMSO in gut [39] and angiogenesis-on-a-chip [40] models. The latter was also used to compare ROS content between quiescent and angiogenic EC to show a low-throughput (LT) application of the assay. With this work we show a new assay to quantify ROS multiplexed with a cell viability readout in physiologically relevant on-a-chip models to use in studies with different throughput.

2. Results

2.1. Short-term exposure and high concentrations of TBHP are required to enhance ROS production

A vasculature-on-a-chip model was used to develop a scalable live-cell image-based scalable assay to quantify intracellular ROS and cell viability. The model consisted of human ECs (HUVEC), cultured against a rat tail collagen I ECM in a tubular structure (Fig. S 1A) which was maintained under gravity driven perfusion [38]. The ROS-viability assay utilizes DHR123, PI, and Hoechst to stain cells for ROS, dead cells, and DNA, respectively. Images of stained cultures were acquired with a HC fluorescence microscope; ROS were quantified based on the fluorescent signal produced by the oxidized version of DHR123, the fluorescent rhodamine 123 (Rh123), normalized against the number of nuclei [41]. Cell viability was determined through the total number of nuclei and of dying cells, stained with Hoechst and PI respectively.

To make the assay scalable, we developed what we termed the top-bottom approach. To acquire the entire micro-vessel more than 30 images of the x-y plane, acquired at different heights along the z-axis (Fig. S 1 B, C), are required. The majority are low-content images, to visualize the side of the micro-vessel (Fig. S 1C) while 6 are high-content images, with the bottom and top of the micro-vessel. The top-bottom approach focused only on these high-content images. We demonstrated (Fig. S 1D, E) that the ROS measured were comparable, in terms of trend and statistics, to the one obtained with the entire micro-vessel. From now on, unless specified, top-bottom approach was used to generate the results.

Different exposure times (0.5, 1, 2 and 5.5 h) and concentrations (0.1, 1 and 10 mM) of TBHP were tested to select the condition for the control which strongly enhances ROS content without affecting cell viability or nuclei counts (Fig. S 2). Overall high concentrations (1 and 10 mM) combined with short-term exposure (0.5 h) were the most effective conditions to enhance ROS production between 10 and 20-fold compared to standard media. On the contrary, the low concentration (0.1 mM) did not induce an effect in ROS content. All conditions did not affect cell viability. Based on these results 0.5 h was selected as the optimal time for control exposure and from now on, unless specified, 0.5 h was used as exposure time.

An NO probe, DAF-FM diacetate (DA), was tested with and without TBHP 1 and 10 mM (0.5 h) to confirm that with TBHP and the assay different redox species are generated rather than ROS. no DAF-FM DA staining was detected (Fig. S 3).

To quantify TBHP EC_{50}, test the assay in accumulation mode, and further optimize the concentration to use as control, 8 concentrations, from 10 μM to 20 mM, were tested (Fig. 1). TBHP treatment caused a clear concentration dependent increase in ROS (Fig. 1A, ROS-green) without affecting dead (Fig. 1A PI-red) or nuclei count (Fig. 1A, DNA-blue). There was a small but significant decrease in the cells count at 3 and 5 mM (Fig. 1B) and no effect for cell viability (Fig. 1C). In terms of ROS content (Fig. 1D) the inefficacy of concentrations below 1 mM was confirmed as well as the strong increase above 1 mM (p-value$<$0.0001). Fluorescence intensity normalized against number of nuclei increases with a sigmoidal trend and a linear range between 1 and 10 mM, where the signal reached the upper plateau (Fig. 1E). The EC_{50} was 4.2 mM and parameters of the fitted equation, are shown in Fig. 1E.

Because cell viability did not decrease over the concentration tested, *trans*-endothelial electrical resistance (TEER) was measured for the same concentrations for 0.5 and 1.5 h exposure (Fig. S 4). Overall, there was a high variability in the response also without treatment, anyway for all concentrations and exposure times TEER decreases but the effect was not dose-dependent.

Taken together 10 mM TBHP was the most effective concentration which can be used as positive control to study ROS accumulation, as cells are still viable after the treatment, TEER is affected as much as with the rest of concentration and its signal is stable and clearly different from any autofluorescence observed in the media control.

2.2. Mitochondrial source of ROS detected in the assay

To exclude that ROS quantified in the assay derived only from mitochondria, Antimycin A and Rotenone were tested separately and in combination (Fig. S 5), together with 10 mM of TBHP for 0.5 h. Rotenone seems to induce a decrease in nuclei count, except for untreated cells, all the treatments induced similar level of ROS, while dead cells were comparable between all conditions (Fig. S 5A). The decrease in nuclei count induced by rotenone 20 μM or in combination with antimycin-A was significantly different compared to untreated culture (p-value = 0.0012 and 0.0436; Fig. S 5B). While the content of ROS (Fig. S 5C) was similar besides the treatment with inhibitors. It was possible to notice that rotenone, alone or with antimycin-A, induced also a change in morphology of the DHR123 staining and tubule seems disrupted.

2.3. ROS depletion assay set-up to screen for antioxidant compounds

After selecting the optimal dose of TBHP to enhance ROS signal we investigated ROS depletion using a dose-response study with curcumin, resveratrol, gallic acid and tocopherol to screen for antioxidants. Between 8 and 9 concentrations of antioxidants were tested to quantify IC_{50} based on ROS signal depletion, and to select a reference control for this set-up. To exclude the possibility that TBHP and the antioxidant reacted in solution with the consequent decrease in concentration of the oxidant (TBHP) applied to the cells, we compared qualitative results from separate and combined exposure of oxidant and antioxidant. In both cases a comparable decrease in the ROS signal compared to the TBHP control could be observed (Fig. S 7). The combined exposure was used for all further experiments.

The highest concentration was determined based on the tolerance of cells to vehicle used to solubilize the antioxidant compound (0.1% for DMSO and 1% for EtOH both v/v). The ranges used were 0.01–67 μM for curcumin, 0.001–1000 μM for resveratrol, 10 pM to 1.1 mM for gallic

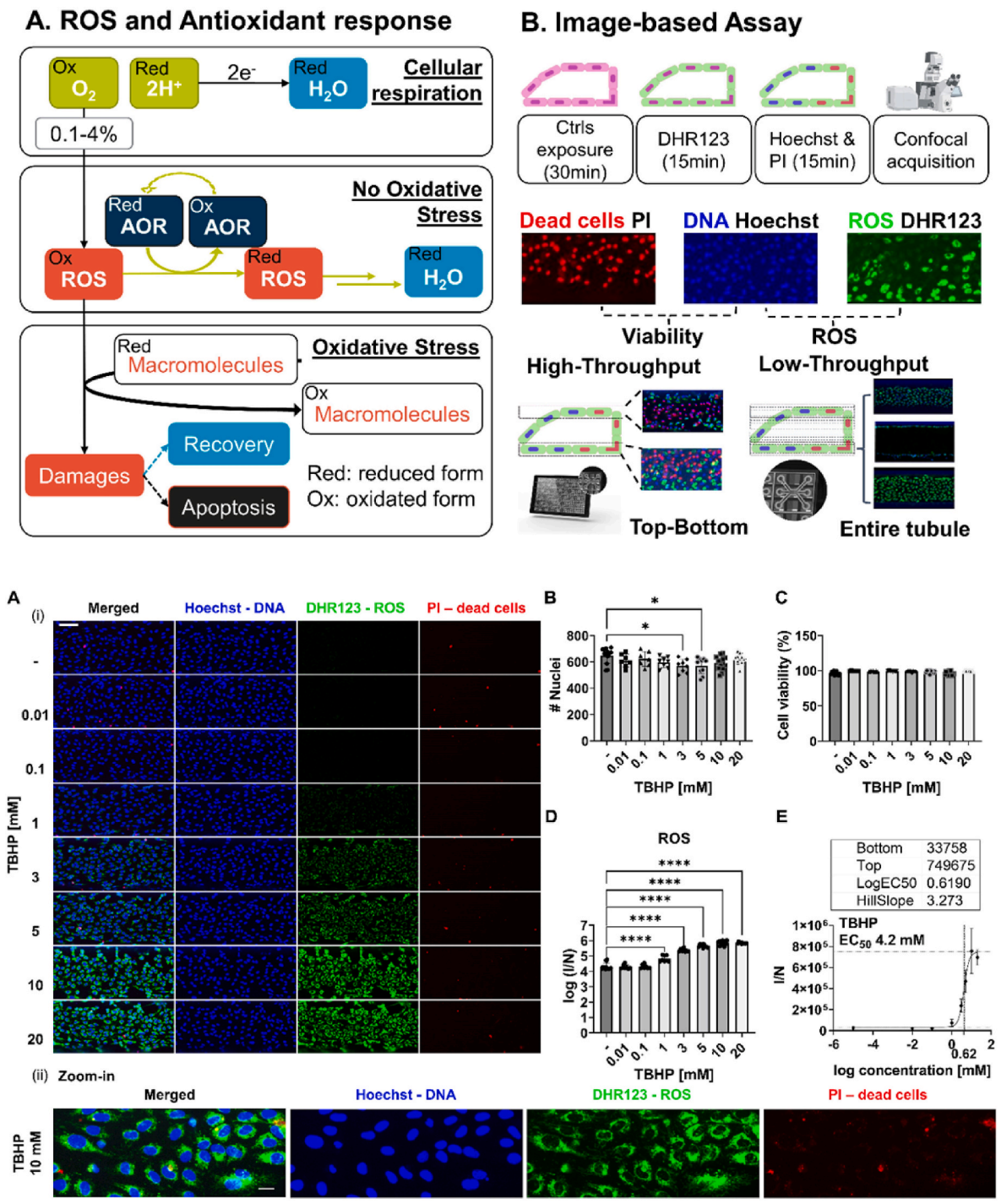

Fig. 1. Accumulation set-up assay. Micro-vessels of HUVECs cultured against ECM, were treated with different concentrations of TBHP (0, 0.01, 0.1, 1, 3, 5, 10 and 20 mM) for 0.5 h and stained for DNA with Hoechst (blue), for ROS with DHR123 (green) and dead cells with PI (red) (A) Representative images of bottom part of the micro-vessel of HUVEC (i) sum-projection of all condition (ii) Max-projection of a part of micro-vessel treated with TBHP 10 mM captured at 20x magnification. Scale bar is 100 μm (i) and 40 μm (ii). Graphs of (B) Cells count (C) cell viability expressed as percentage (D) ROS content in a log scale expressed as fluorescence intensity normalized against the number of cells count (E) Non-linear regression analysis on ROS level over log scale concentration of TBHP. The table above the graph includes information of the model to fit the data. Data are expressed as average ± standard deviation (STD) with N = 3 and n = 2–10 replicates. Difference between results were evaluated by one-way ANOVA with Tukey's multiple comparison (graph in B) or Dunnett's test (graph in D). P-value < 0.05 was considered statistically significant * $p < 0.05$, **** $p < 0.0001$. (For interpretation of the references to color in this figure legend, the reader is referred to the Web version of this article.)

acid and 0.001–10000 μM for tocopherol. Images of chips cultured in standard media, which in this set-up act as positive control, were used to qualitatively ensure that the culture was healthy, (Fig. 2A). Both cell viability (Fig. 2B) and ROS content (Fig. 2C) are expressed as percentage, for ROS, 100% is the negative control (TBHP) and 0% is the vehicle control.

Based on the images, except for tocopherol, the rest of the compounds (Fig. 2A) showed a concentration dependent decrease in ROS. While there was no effect for cell viability (Fig. 2B). To compare the potency between antioxidants to reverse ROS accumulation we

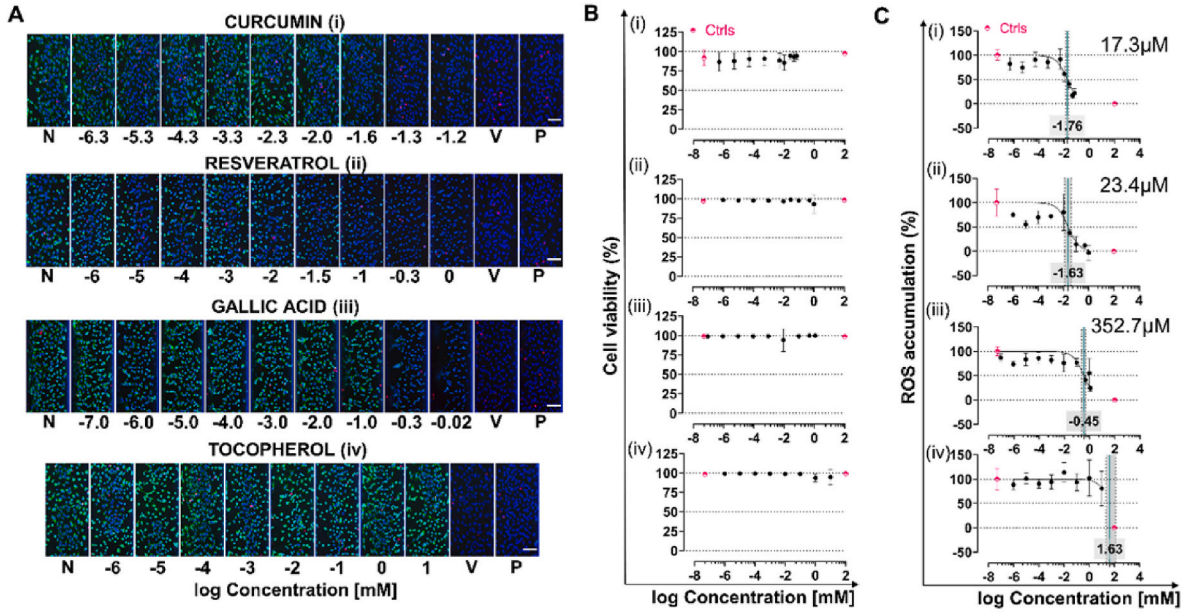

D

	SET-UP ASSAY	
CONTROLS	**Accumulation**	**Depletion**
Negative (N)	Media/Vehicle (V)	TBHP 10 mM
Positive (P)	TBHP 10 mM	Media/Vehicle
Reference (R)		TBHP 10 mM + Curcumin 67 μM

Fig. 2. Depletion assay set-up. Micro-vessel of HUVEC, cultured as micro-vessel in the OrganoPlate 3-lane 40 against the ECM, were treated for 30 min simultaneously with TBHP (10 mM) and different concentrations of antioxidants: curcumin (i), resveratrol (ii), gallic acid (iii) and tocopherol (iv). The culture was stained for DNA with Hoechst (blue), for ROS with DHR123 (green) and dead cells with PI (red) (A) Representative images of sum-projection of bottom part of the micro-vessel. N indicates negative, V vehicle and P positive control. (B) Cell viability over concentration of antioxidant. (C) Dose-response curve of ROS content expressed as percentage with 0% indicating vehicle control and 100% negative control, against concentration of antioxidants in log scale. IC_{50} values, quantified based on the ROS depletion, are indicated in each graph as a green line with confidence interval (95% grey area delimited by dotted lines) and as a number. Data are expressed as average ± STD, data in pink are N (on the left) and V (on the right) controls and data in black are samples data (D) Table with the different controls selected per set-up of assay. Data are expressed as average ± STD and in terms of replicates for curcumin N = 3, n = 2–4, for gallic acid n = 2–5, for tocopherol n = 1–5 and for resveratrol N = 2 and n = 1–5. All scale bars are 100 μm. (For interpretation of the references to color in this figure legend, the reader is referred to the Web version of this article.)

quantified the IC_{50} (Fig. 2C) which was in the range of μM for all except for tocopherol (n.d.). Curcumin was the most potent with an IC_{50} of 17.3 μM (13.3–22.5 CI 95%), followed by resveratrol with 23.4 μM (12.8–41.8 CI 95%) and gallic acid with 352.7 μM (236–516.6 CI 95%). Based on these results as reference control condition we selected the highest concentration of curcumin (67 μM) and TBHP (10 mM). Taken together these results show that the assay can be used to measure ROS depletion and is sensitive enough to measure over a range of concentrations. Importantly the setup was validated using multiple antioxidants.

2.4. Higher baseline level in Caco2 cell line and the barrier integrity is affected

Our results so far indicate that the assay can be used both to study accumulation and depletion of intracellular ROS together with cell viability in vasculature-on-a-chip models. To validate the assay and show its application to characterize on-a-chip models, selected controls (see Fig. 2D) were tested in gut-on-a-chip model (Fig. 3) [39]. Also in this model Caco2 were culture with a tubular structure against ECM, under perfusion (Fig. 3A). Gut-on-a-chip showed 3-fold and 4-fold higher baseline of ROS with media and DMSO respectively (Fig. 3B) compared to what generally found with vasculature-on-a-chip, but overall the trend between controls and the effect on cell viability (Fig. 3C) were the same.

As we did for the vasculature model, the effect of TBHP was tested on the barrier integrity by measuring TEER (Fig. S 6) over the same concentrations (10 μM–20 mM) and exposure time (0.5 and 1.5 h) used with HUVEC. For short exposure time and concentration above 1 mM there was a decrease which did not depend on dose and the TEER was still above the 50% of the effect. For longer exposure for 1 mM and higher concentration the drop in TEER was drastic (p-value < 0.0001).

Overall the assay is validated to be used in accumulation and depletion with gut-on-a-chip model and we showed that Caco2 cells present a higher level of ROS compared to HUVEC and short exposure time are crucial to not compromise the integrity of gut-on-a-chip barrier.

2.5. Differences in ROS levels between angiogenic and quiescent ECs

The assay was further validated in angiogenesis on-a-chip models (Fig. 4) [40], established by stimulating a micro-vessel to generate perfusable sprouts in the adjacent microfluidic channel with ECM, by adding a solution of pro-angiogenic factors [42] to the channel opposite to the micro-vessel. As with the vasculature-on-a-chip also in this model (Fig. 4A), no accumulation was registered with media and DMSO, TBHP enhanced almost 20-fold ROS content compared to media, and curcumin-TBHP was in between (Fig. 4B). While for the cell viability (Fig. 4C) there was a small difference with TBHP treatment even if it was still reasonably high.

To show a LT application of the assay, the entire Z-stack was acquired, to characterize the model in detail. ROS content was quantified in 2 different areas: in the micro-vessel, which contains quiescent ECs, and in the sprouts area, which contains angiogenic ECs. In Fig. 4D in media, DMSO and curcumin-TBHP treatment condition there is a

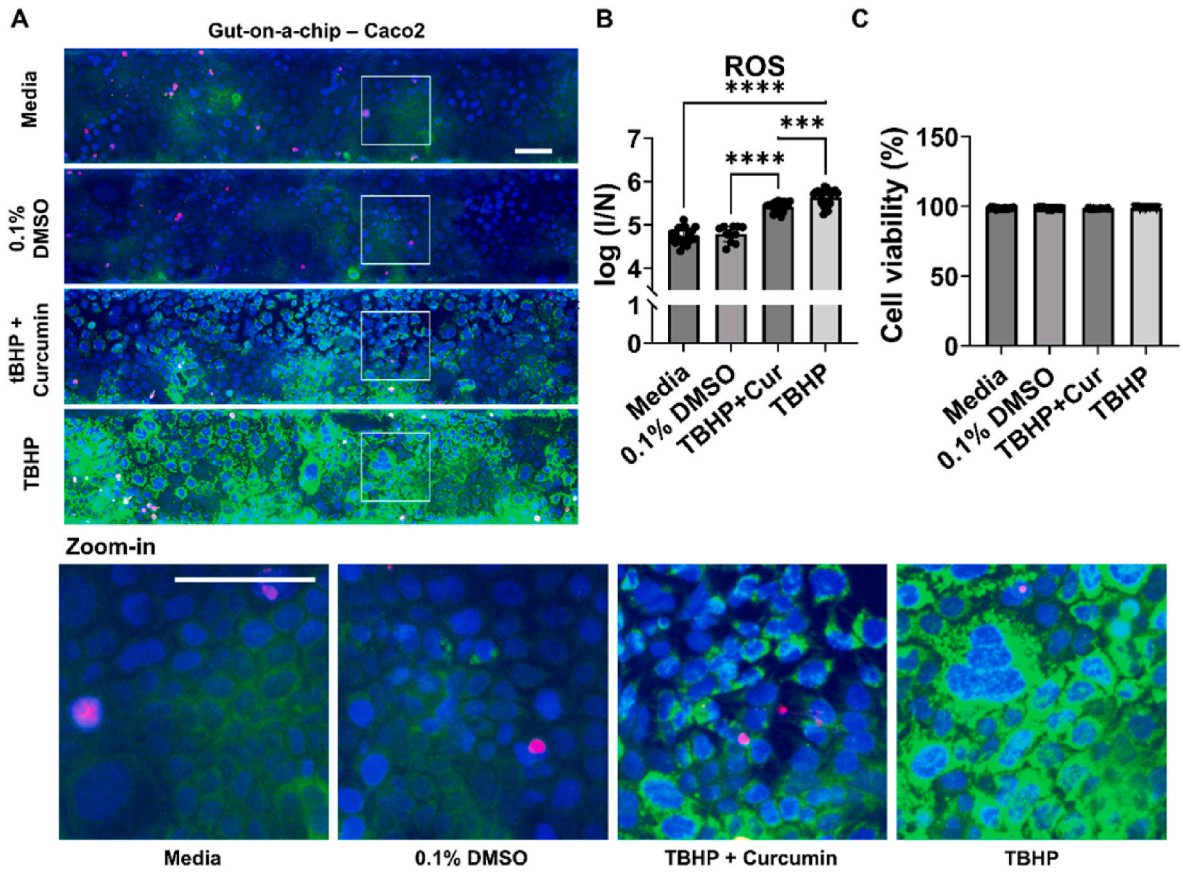

Fig. 3. Application and validation of multiplex ROS-cell viability assay for HT studies in gut-on-a-chip model with Caco2 cultured as a tubule in the OrganoPlate 3-lane 40 against ECM. Gut-on-a-chip models were treated with standard media or 0.1% of DMSO or TBHP 10 mM with and without curcumin 67 μM, and stained for DNA with Hoechst (blue), for ROS with DHR123 (green) and dead cells with PI (red) (A) Representative sum-projection images of bottom part of tubule of Caco-2 with a zoom-in on the cells below. (B) ROS content in a log scale expressed as fluorescence intensity normalized against the number of cells count (C) Cell viability expressed as percentage. Data are expressed as average ± STD and derived from 3 separate experiments (N = 3) with n = 3–7. Difference between results were evaluated by one-way ANOVA with Tukey's multiple comparison. P-value < 0.05 was considered statistically significant ***p = 0.0003, ****p < 0.0001. All scale bars are 100 μm. (For interpretation of the references to color in this figure legend, the reader is referred to the Web version of this article.)

slightly stronger ROS signal in the angiogenic ECs compared to quiescent ECs. This increase in ROS was also significantly different between angiogenic and quiescent ECs with all conditions and except for DMSO (p-value = 0.0024), the rest had a p-value lower than 0.0001 (Fig. 4E).

Taken together we validate the assay also for angiogenesis-on-a-chip models and show a different application in LT context where it was possible to capture different ROS level in quiescent and angiogenic ECs.

3. Discussion

The quantification of ROS production is generally conducted in 2D *in vitro* cell culture due the limitations of quantifying ROS *in vivo*, where they are estimated by indirect measurements. The creation of new *in vitro* models that are more complex and resemble more physiologically relevant environments requires an adaption of assays to measure ROS. In the majority of the 2D studies which quantify ROS, cell viability is also monitored. Monitoring ROS in complex 3D models which can concurrently measure pathophysiology adaptations will provide a way to help decipher how oxidative stress regulates mechanistic pathways and pave the way to develop new therapeutics. With this in mind, we developed a scalable multiplex versatile image-based assay to quantify intracellular ROS and cell viability in organ-on-a-chip models with a tubular structure.

In order to achieve scalability certain levels of resolution were sacrificed like with the top-bottom approach which utilize only a part of the tubule to drastically speed up the acquisition and reduce the amount of data to store, which is a critical parameter for HT application like screening. Fluorescence microscopy was selected as technique because it is both multiplex and scalable friendly as it is used for high-content screening. The choice of multiplexing ROS with cell viability was made to understand the degree of the OS insult. As probe to stained for DNA, ROS and dead cells we opted for Hoechst, DHR123 and PI. DHR123 was selected because the intracellular loss of Rh123, a positively charge and lipophilic molecule, is much lower compared to DFCDA [43], another extensively used probe. It is important that the DHR123 probe does not leak out from cells, as incubation time can last for 30mins before measurements obtained. To develop the assay we used a vasculature model as it is the system which can well recapitulate ROS as signaling or damaging molecules [44].We chose angiogenesis and gut model to validate the assay as the first one has a different 3D structure compared to vasculature model and the second one is a different organ.

The assay was also designed to be versatile, to study ROS accumulation and depletion and so controls were optimized to maximize the separation between the highest and the lowest signal. As a control to induce ROS, we used *tert*-butyl hydroperoxide ($(CH_3)_3CO_2H$ TBHP) because it is chemically similar to hydrogen peroxide but more stable and it was already used to induce OS in previous studies [45–51]. The assay showed to be reliable to be performed in accumulation (Fig. 1) and depletion (Fig. 2) set-up. As control condition to enhance ROS without affecting cell viability short-exposure time and high concentration were selected. High concentration was expected as generally used with organ-on-a-chip models to induce ROS [29,30,52,53]. Short-term

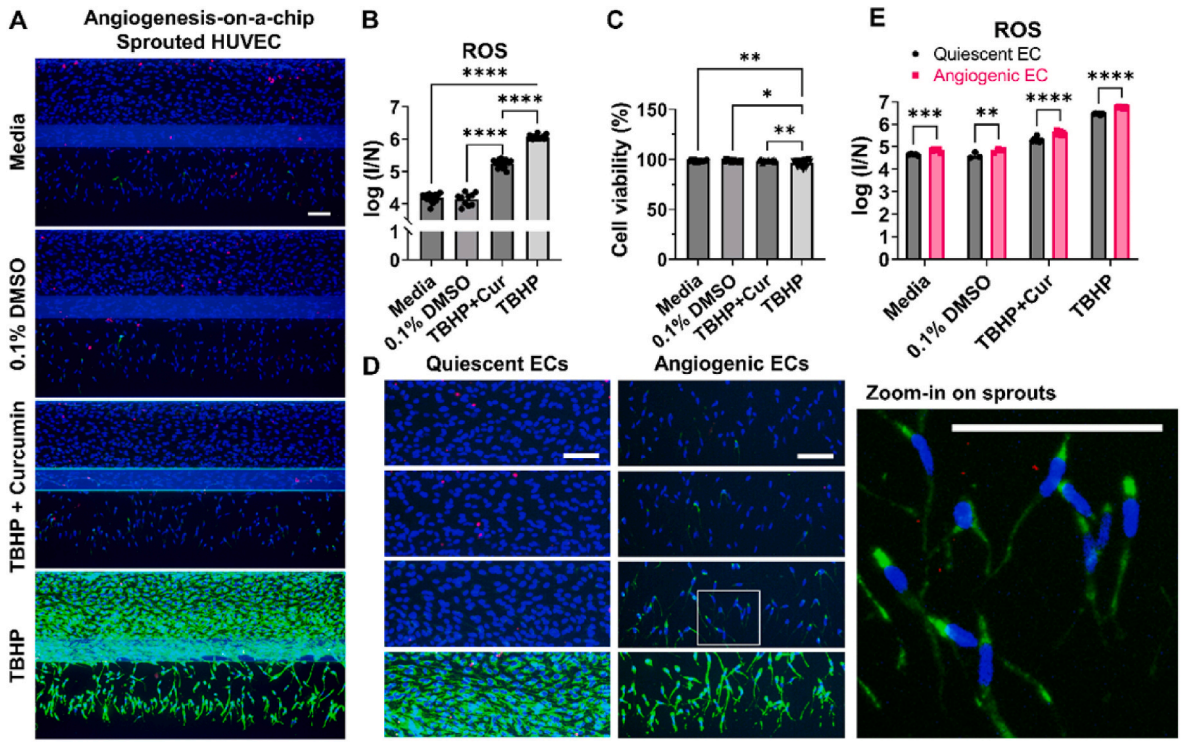

Fig. 4. Application and validation of multiplex ROS-cell viability assay for HT and LT application on angiogenesis-on-a-chip. Micro-vessels of HUVECs cultured against ECM under perfusion and stimulated to generate sprouts were treated with TBHP 10 mM with and without curcumin 67 μM, standard media or 0.1% of DMSO and stained for DNA with Hoechst (blue), for ROS with DHR123 (green) and dead cells with PI (red) (A) Representative images of max-projection of entire micro-vessel (B) ROS content in a log scale expressed as fluorescence intensity of DHR123 normalized against the number of cells count (C) Cell viability expressed as percentage (D) LT application on angiogenesis-on-a-chip: representative images of max-projection of entire Z-stack of quiescent (micro-vessel) and angiogenic (sprouts) ECs. Zoom-in on the angiogenic part of the angiogenesis-on-a-chip model treated with 10 mM of TBHPTBHP and 67 μM of curcumin (E) ROS content in angiogenic and quiescent ECs, expressed as ratio between ROS fluorescence intensity and nuclei count in a log scale. Data are expressed as average ± STD and in terms of replicates graph in (B) and (C) N = 3 and n = 2–7 while graph in (E) N = 1 and n = 3–7. Difference between results in graph (B) and (C) were evaluated by one-way ANOVA with Tukey's multiple comparison P-value < 0.05 was considered statistically significant * p = 0.0245, **p = 0.0014, ****p < 0.0001. While in graph (E) two-way ANOVA with Sidak's test was used to compare ROS content in angiogenic and quiescent ECs, p-value < 0.05 was considered statistically significant **p = 0.0024, *** = p = 0.0009 ****p < 0.0001. All scale bars are 100 μm. (For interpretation of the references to color in this figure legend, the reader is referred to the Web version of this article.)

exposure were also expected to avoid affecting cell viability, in fact previous studies run in 2D with HUVEC, showed that for exposure of 1 h, TBHP did not induce a decrease below 50% up to 500 μM [48], and for long-term exposure of 6 h the IC_{50} was generally in a range of hundreds of μM [49,51].

The signal generated by TBHP treatment and detected by DHR123 staining seems specific for ROS and not include RNS, as a NO specific probe did not yield staining (Fig. S 3). Furthermore, the DHR123 signal was attenuated with antioxidant treatment (Fig. 2). The exact source of ROS was not confirmed based on the location and shape of the DHR123 staining it is likely that (Fig. 1A(ii)) it is both from mitochondria and endoplasmic reticulum. However the TBHP-induced ROS signal was not affected by inhibitors of mitochondrial respiratory chain complexes I and III (Fig. S 5). A possible explanation is that mitochondria contribute with other complexes, or that ROS detected in the assay derive from a secondary reaction of the ROS directly produced from mitochondria.

As we expected high concentration to induce ROS we hypothesize the same for antioxidants to reverse the effect, based on 2D literature, where generally the same magnitude of concentration is applied for oxidant and antioxidant [49,51]. On the contrary with vasculature-on-a-chip much lower concentrations of antioxidant compared to TBHP (x100 less, Fig. 2) are effective to reverse the effect, indicating that cells are more prone to scavenge ROS rather than accumulate them. These results also suggest that on-a-chip culture are less prone to experience OS than 2D as which was previously shown by a direct comparison of level of metabolic products induced by OS in on-a-chip and 2D culture [54]. This difference in level of ROS accumulated and in experiencing OS between 2D and on-a-chip could be explained by the presence of physiological features absent in 2D such as the flow which has already been reported to affect the way cells experience OS, and accumulate ROS [55].

By confirming the overall trend between controls found with the vasculature model we validated the assay with gut (Fig. 3) and angiogenesis-on-a-chip models (Fig. 4). We also showed the capability of the assay to distinguish between different ROS content in different types or phenotypes of cells. The fact that higher level of ROS was detected in untreated Caco2, a cell line isolated from tissue affected by colorectal adenocarcinoma, compared to untreated HUVEC, which are primary cells, indicates that the assay can capture different ROS for tumor or normal cells. It can also distinguish between different level of ROS in physiological processes as with the angiogenesis-on-a-chip model (Fig. 4E) where sprouts have higher level of ROS compared to quiescent ECs. Higher level of ROS in certain physiological and pathological processes, such as cancer and angiogenesis [44], have already been shown but generally not with a direct quantification of ROS, in a highly physiologically relevant *in vitro* model.

In conclusion, we developed a scalable, sensitive, versatile, multiplex image-based ROS-viability assay to use with organ-on-chip models. We showed that the assay is reliable and versatile as it can be used to detect inhibition or stimulation of ROS content and is validated with epithelial and endothelial cells. It is sensitive enough to distinguish between different ROS level of physiological processes such as in migrating

endothelial cells in an angiogenesis-on-a-chip model and to capture higher level in pathological cells. Taken together the application of this assay could help understanding mechanism of redox signaling, developing models with the right OS profile and screen for new antioxidant therapeutics.

4. Material and methods

4.1. Reagents and cell

Primary human umbilical vein endothelial cells (HUVECs from Lonza, #C2519AS), EBM-2 medium (Lonza, #CC-3156), supplemented with EGM-2 SingleQuots (Lonza, #CC-4176), Human epithelial colorectal adenocarcinoma cells (Caco2 from Sigma-Aldrich, #86010202), rat tail collagen I (Corning, #354249), Acetic acid (Sigma-Aldrich, #A6283, ≥99%), HEPES buffer saline solution (Lonza, #CC-5024), sodium bicarbonate ($NaHCO_3$ from Sigma-Aldrich, #S5761), Hanks' Balanced Salt Solution (HBSS from Gibco, #55037C), Phosphate-Buffered Saline (PBS from Gibco, #70013065), Vascular Endothelial Growth Factor (VEGF rhVEGF-164 PeproTech, #100-20-1 mg), Sphingosine-1-phospate (S1P from Sigma-Aldrich, #73914), Phorbol myristate acetate (PMA from Sigma Aldrich, #P1585-1 MG), Dimethylsulfoxide (DMSO from Sigma Aldrich, #D8418), Ethanol absolute (VWR, #BAKR8025.2500), MilliQ water (Obtained with Millipore Vent filter 12FC ZFRE012FC), *tert*-butyl hydroperoxide solution (TBHP from Sigma, #458139, 70% in H2O w/w), Dihydrorhodamine 123 (DHR123 from Sigma-Aldrich, #D1054), Hoechst 33342 (ThermoFisher, #H3570, 10 mg/mL in H2O), Propidium Iodide (PI from ThermoFisher, #P3566, 1 mg/mL in H2O), 3,4,5-Trihydroxybenzoic Acid Hydrate (Gallic acid hydrate from TCI, #G0011), 3,4′,5-Trihydroxy-trans-stilbene (Resveratrol from Sigma Aldrich, #R5010), (E,E)-1,7-Bis(4-hydroxy-3-methoxyphenyl)-1,6-heptadiene-3,5-dione (Curcumin from TCI, #C0434), (±)-α-Tocopherol (Sigma Aldrich, #T3251), 4-Amino-5-methylamino-2′,7′-difluorofluorescein diacetate (DAF-FM DA from Sigma-Aldrich, #D2321, 5 mM in DMSO), Rotenone (Sigma-Aldrich, #R8875), Antimycin A from Streptomyces sp. (Sigma-Aldrich, #A8674).

4.2. Microfluidic cell culture

We used the OrganoPlate 3-lane 40 (4004-400B, MIMETAS BV) to establish the organ-on-a-chip cultures. A plate comprises 40 microfluidic chips printed on image quality glass on the back of a 384 micro-titer well plate. Each chip includes 3 channels, the middle one, called the gel channel, is generally filled with ECM and the other two, called perfusion channels, are used to culture cells with a tubular structure. Each channel has dedicated inlets and outlets. There are two phaseguides™ to separate the channels and culture cells in direct contact with ECM in a barrier free system [56]. The culture is maintained under a gravity driven perfusion by using the Organoflow® (MIMETAS BV) a customized rocking platform. For all models used in this work the perfusion setting were 7° and 8 min interval. In all the experiments ECM and cells seeding were handled by a pipetting robot (Biomek i5, Beckman Coulter).

4.3. Vasculature-on-a-chip

To establish the vasculature-on-a-chip HUVEC culture against Collagen I were used. To prepare the ECM Collagen I (20 mM in acetic acid), was diluted to 7.5 mg/ml, mixed with 1 M HEPES and 37 g/L $NaHCO_3$ (ratio 8:1:1), and 2 μL were dispensed in the middle channel of the chips. ECM was left polymerize in a cell culture incubator at 37°C with 5% CO_2 for 15 min and then hydrated by adding 30 μL HBSS to the inlet of the middle channel and 3 μL HBSS to inlets of both perfusion channels. OrganoPlates were placed back in the incubator for 24 h and then HUVEC in EGM-2 media were seeded in the top perfusion channel with a cell density of ~8000 cells/μL. To seed the cells we used the method of passive pumping as already described in the literature [57]. We aspirated HBSS from the inlets of the middle channel. A volume of 50 μL EGM-2 medium was added to the inlet of the top perfusion channel and a droplet of 1.25 μL HUVECs was added to the corresponding outlet to attain 10000 cells/chip.

The OrganoPlates were placed at 75° degree angle using a holder inside a cell culture incubator at 37°C with 5% CO_2 to allow HUVECs to attach to ECM in the middle channel. After 2.5 h 50 μL EGM-2 medium was added to the outlets of the top perfusion channels. The OrganoPlates were placed back in the cell culture incubator on an OrganoFlow. It took 2 days to develop stable micro-vessels, medium was replaced every 2 days and only in the top perfusion channel. Assays were performed from day 2.

4.4. Angiogenesis-on-a-chip

To establish angiogenesis-on-a-chip vasculature-on-a-chip was cultured for 3 days before applying a mixture of growth factors to stimulate sprouts. The mixture was prepared with 50 ng/mL of VEGF, 50 nM of Sphingosine-1-Phosphate, and 2 ng/mL of PMA in EGM-2 [42]. The mixture was added to the bottom channel opposite to the one with cells and refreshed every other day as well as EGM-2 media in the top perfusion channel. Assays were run from day 6 when sprouts were completely formed.

4.5. Gut-on-a-chip

To establish the gut-on-a-chip Caco-2 culture against Collagen I were used. To seed ECM and cells, we followed the same procedure as for the vasculature-on-a-chip, with the differences that cells were seeded directly after ECM polymerization, in EMEM medium (with 10% FBS heat-inactivated (HI), 1% nonessential amino acids, 1% penicillin–streptomycin (10,000 U/ml)) with a cell seeding density of 10000 cells/μL to obtain 12500 cells/chip. Medium was added in top and bottom perfusion channels and refreshed it every other day. Assays were performed from day 5.

4.6. Multiplexing ROS and cell viability assay

4.6.1. ROS-cell viability accumulation set-up

The assay consists in a series of exposures and washing steps. For each step unless otherwise specified, 50 μL of solution are added in each inlet and outlet of the channel with cell (100 μL/chip). For all the washing steps the following scheme was used: all inlet and outlets were aspirated, 100 μL of HBSS were added in the inlet of the top channel and 50 μL in the rest of the in/outlet wells (400 μL/chip). As a first step, culture was exposed to controls (see table in Fig. 2D) for 0.5 h. A washing step was performed, followed by a 15 min incubation of a solution of DHR123 (5 μM,from stock solution of 5.8 mM in DMSO, *~0.5 pmol/cell)* in standard culture media to stain for ROS. Two washing steps were performed before the last exposure of 15 min to a solution of Hoechst 33342 (0.005 mg/mL diluted from stock solution of 10 mg/mL in water) and PI (0.005 mg/mL from stock solution of 1 mg/mL in water) in HBSS to stain for DNA and dead cells, respectively. All incubations were performed in a cell culture incubator at 37°C with 5% CO_2. An ImageXpress confocal microscope was used to acquire images of the micro-vessel at 10x magnification, unless specified. DAPI (Ex/Em: 359/461 nm), FITC (Ex/Em: 490/525 nm) and TexasRed (Ex/Em: 595/620 nm) were acquired.

4.7. ROS-cell viability depletion set-up

The assay works as in the accumulation set-up the only difference is in the type of controls (see table in Fig. 2D) and to that during the first exposure the culture was simultaneously exposed to 10 mM TBHP together with the compounds under investigation. For the remaining steps we followed the same scheme as for the accumulation set-up. To

test the assay we used 4 antioxidant compounds curcumin, resveratrol, gallic acid and tocopherol. Curcumin, resveratrol, gallic acid and tocopherol stock solution were made in absolute ethanol or DMSO and the sample diluted to obtained the different concentration in standard media.

4.8. High-throughput (HT) application

For HT application we used the top bottom approach where we acquired and analyzed only 3 z-slices (z-step increment of 5 μm) of the top and of the bottom of the micro-vessel. To acquire an entire plate in around 6–8min instead of 40, and to work with light file (~4 GB instead of ~35).

4.9. Low-throughput (LT) application

For LT application we acquired the entire z-stack (33 z-slices, with a Z-step increment of 5 μm) but for a small amount of chips (max 8 at the time).

4.10. Control optimization

Vasculature-on-a-chip models were exposed to 0, 0.1, 1 and 10 mM of TBHP in EGM-2 media for 0.5, 1, 2 and 5.5 h. The multiplex assay (ROS and cell viability) in accumulation set-up for HT application was used. Once selected 0.5 h as exposure time a calibration curve was realized by exposing vasculature model to 0, 0.01, 0.1, 3, 5, 10 and 20 mM of TBHP in standard culture media.

4.11. NO quantification with DAF-FM DA

Vasculature-on-a-chip models were exposed to TBHP 1 and 10 mM TBHP or standard culture media for 0.5 h. As for the ROS-cell viability assay, for each step unless otherwise specified, 50 μL of solution were added in each inlet and outlet of the channel with cell (100 μL/chip). For all the washing steps the following scheme was used: all inlet and outlets were aspirated, 100 μL of HBSS were added in the inlet of the top channel and 50 μL in the rest of the in/outlet wells (400 μL/chip).

Cells were washed with HBSS and exposed to DAF-FM DA 1 μM (from stock solution of 5 mM in DMSO) for 15 min (100 μL per chip), washed twice with HBSS and the exposed stained for DNA. All incubations were performed in a cell culture incubator at 37°C with 5% CO_2. An ImageXpress confocal microscope was used to acquire images of the micro-vessel at 10x magnification, unless specified. DAPI (Ex/Em: 359/461 nm), FITC (Ex/Em: 490/525 nm) and TexasRed (Ex/Em: 595/620 nm) were acquired.

4.12. Barrier integrity measurement with TEER

Vasculature-on-a-chip and gut-on-a-chip models were exposed to TBHP 0.01, 0.1, 3, 5, 10 and 20 mM or standard culture media for 0.5 h under perfusion in a cell culture incubator at 37°C with 5% CO_2. Treatment solutions were replaced in all the inlet and outlet well of the OrganoPlate with standard culture media and the plate was left for 0.5 h at room temperature before performing the TEER measurement. In parallel electrodes were sprayed with 70% EtOH and left dry out for 0.5 h, before starting the first measurement. Standard media was removed and the TBHP treatments replace for an additional exposure of 1 h, and a second measurement was repeated in same way as the first one.

4.13. Inhibitors of electron chain reaction

Vasculature-on-a-chip cultures were exposed to 10 mM TBHP with and without antimycin (5 and 10 μM), rotenone (20 and 40 μM), rotenone (40 μM) together with antimycin (10 μM) or standard media for 0.5 h, we followed the procedure for the depletion set-up assay for HT application.

4.14. ROS depletion assay set-up application

Vasculature-on-a-chip models, were exposed to 4 different antioxidants: curcumin (67, 45, 25,10, 5, 0.5, 0.05, 0.005 and 0.0005 μM dilutions prepared from a stock solution of 67 mM in DMSO), resveratrol (1000, 500, 100, 30, 10, 1, 0.1, 0.01 and 0.001 μM dilutions prepared from a stock solution of 219 mM in EtOH), gallic acid (1128, 940, 470, 94, 9, 0.9, 0.09, 0.009, 0.0009, 0.00009 μM dilutions prepared from a stock solution of 94 mM in EtOH) and tocopherol (10, 1, 0.1, 0.01, 0.001, 0.0001, 0.00001, 0.000001 μM dilutions prepared from 100% tocopherol). Once established the vasculature we exposed the culture to Curcumin, Resveratrol, Gallic acid or tocopherol together with TBHP and we followed the procedure for the depletion set-up assay for HT application. In this assay set-up 10 mM TBHP acted as negative control, 0.1% DMSO or 10 %EtOH as vehicle controls, depending on the vehicle used to dissolve the antioxidants and standard EGM-2 media as positive control.

4.15. Assay validation with angiogenesis and gut-on-a-chip

To validate the assay, we tested the controls selected for accumulation and depletion set-up (table in Fig. 2D) which were standard media, 0,1% DMSO, 67 μM Curcumin +10 mM TBHP (curcumin-TBHP) and 10 mM TBHP in gut and angiogenesis-on-a-chip. For both model we applied the HT application and for a subset of the angiogenesis data we used the LT application.

4.16. Data analysis & statistics

Raw data were processed in imageJ/FIJI where we made montages of each channels. Images on DAPI and TexasRed channel were used to quantify the nuclei count of live and dead cells. Images on FITC channel were used to quantify fluorescence intensity. For both quantification we used two macro developed in-house. Data were analyzed in excel to express ROS content and cell viability. ROS content was quantified with fluorescence intensity normalized against nuclei count. We always include a cell free chip to subtract intensity of background. Values are given as average ± standard deviation. Data were generated in at least 2 independent experiments, unless specified. The notation "N" indicates number of independent experiments, while "n" number of chip per condition per independent experiment. Statistical analyses were performed with Graphpad. Multiple comparisons were made by 1-way ANOVA followed by Tukey's or Dunnett's multiple comparison test or by 2-way ANOVA followed by Dunnett's or Sidak's test, as specified in the legend or in the graphs. P-values are specified in the legend of each graph.

Author contributions

C. Soragni designed the study, performed experiments, data analysis and drafted the first draft of the manuscript. C. Ping Ng, Colin E. Murdoch, L.J. de Windt edited the first draft. C. Ping Ng, Colin E. Murdoch, L.J. de Windt and J.S. Trietsch supervised the research. C. Soragni, G. Rabussier, C. Ping Ng, H.L. Lanz and K. M. Bircsak contributed to the visualization. All authors read and approved the final manuscript.

Declaration of competing interest

C. Soragni, G. Rabussier, K. Bircsak, H.L. Lanz, S.J. Trietsch and C. P. Ng, are employees of MIMETAS BV, The Netherlands which produces OrganoPlate™, OrganoTEER™ and OrganoFlow™.

Acknowledgements

This work was supported by the European Union's Horizon 2020 research and innovation programme under the Marie Skłodowska-Curie grant agreement No 765274, project iPLACENTA.

Appendix A. Supplementary data

Supplementary data to this article can be found online at https://doi.org/10.1016/j.redox.2022.102488.

References

[1] R.L. Auten, J.M. Davis, Oxygen toxicity and reactive oxygen species: the devil is in the details, Pediatr. Res. 66 (2) (2009) 121–127, https://doi.org/10.1203/PDR.0b013e3181a9eafb.
[2] H. Sies, et al., Defining roles of specific reactive oxygen species (ROS) in cell biology and physiology, Nat. Rev. Mol. Cell Biol. (2022), 0123456789, https://doi.org/10.1038/s41580-022-00456-z.
[3] I. Dalle-Donne, R. Rossi, R. Colombo, D. Giustarini, A. Milzani, Biomarkers of oxidative damage in human disease, Clin. Chem. 52 (4) (2006) 601–623, https://doi.org/10.1373/clinchem.2005.061408.
[4] A.T. Diplock, Antioxidants and disease prevention, Mol. Aspect. Med. 15 (4) (1994) 293–376, https://doi.org/10.1016/0098-2997(94)90005-1.
[5] S. Fuloria, et al., Comprehensive review of methodology to detect reactive oxygen species (Ros) in mammalian species and establish its relationship with antioxidants and cancer, Antioxidants 10 (1) (2021) 1–35, https://doi.org/10.3390/antiox10010128.
[6] M. Schieber, N.S. Chandel, ROS function in redox signaling and Oxidative Stress, Curr. Biol. 100 (2) (2012) 130–134, https://doi.org/10.1016/j.cub.2014.03.034.
[7] P.D. Ray, B.W. Huang, Y. Tsuji, Reactive oxygen species (ROS) homeostasis and redox regulation in cellular signaling, Cell. Signal. 24 (5) (2012) 981–990, https://doi.org/10.1016/j.cellsig.2012.01.008.
[8] A. Lermant, C.E. Murdoch, Cysteine glutathionylation acts as a redox switch in endothelial cells, Antioxidants 8 (2019) 315, https://doi.org/10.3390/antiox8080315.
[9] R.Z. Zhao, S. Jiang, L. Zhang, Z. Bin Yu, Mitochondrial electron transport chain, ROS generation and uncoupling (Review), Int. J. Mol. Med. 44 (1) (2019) 3–15, https://doi.org/10.3892/ijmm.2019.4188.
[10] H. Sies, Hydrogen peroxide as a central redox signaling molecule in physiological oxidative stress: oxidative eustress, Redox Biol. 11 (November 2016) 613–619, https://doi.org/10.1016/j.redox.2016.12.035, 2017.
[11] R. Ray, et al., Endothelial Nox4 NADPH oxidase enhances vasodilatation and reduces blood pressure in vivo, Arterioscler. Thromb. Vasc. Biol. 31 (6) (2011) 1368–1376, https://doi.org/10.1161/ATVBAHA.110.219238.
[12] Y.J. Huang, G.X. Nan, Oxidative stress-induced angiogenesis, J. Clin. Neurosci. 63 (2019) 13–16, https://doi.org/10.1016/j.jocn.2019.02.019.
[13] Y.W. Kim, T.V. Byzova, Oxidative stress in angiogenesis and vascular disease, Blood 123 (5) (2014) 625–631, https://doi.org/10.1182/blood-2013-09-512749.
[14] A. Ozcan, M. Ogun, Biochemistry of reactive oxygen and nitrogen species, in: Basic Principles and Clinical Significance of Oxidative Stress, 2015, pp. 37–58, https://doi.org/10.5772/61193.
[15] C.E. Murdoch, et al., Role of endothelial Nox2 NADPH oxidase in angiotensin II-induced hypertension and vasomotor dysfunction, Basic Res. Cardiol. 106 (4) (2011) 527–538, https://doi.org/10.1007/s00395-011-0179-7.
[16] R.A. Cohen, et al., Endothelial cell redox regulation of ischemic angiogenesis Richard, J. Cardiovasc. Pharmacol. 67 (6) (2016) 458–464, https://doi.org/10.1097/FJC.0000000000000381.
[17] R. Stocker, J.F. Keaney, Role of oxidative modifications in atherosclerosis, Physiol. Rev. 84 (4) (2004) 1381–1478, https://doi.org/10.1152/physrev.00047.2003.
[18] C.E. Murdoch, et al., Endothelial NADPH oxidase-2 promotes interstitial cardiac fibrosis and diastolic dysfunction through proinflammatory effects and endothelial-mesenchymal transition, J. Am. Coll. Cardiol. 63 (24) (2014) 2734–2741, https://doi.org/10.1016/j.jacc.2014.02.572.
[19] M.C. Haigis, B.A. Yankner, The aging stress response, Mol. Cell 40 (2) (2010) 333–344, https://doi.org/10.1016/j.molcel.2010.10.002.
[20] T.M. Paravicini, R.M. Touyz, Redox signaling in hypertension, Cardiovasc. Res. 71 (2) (2006) 247–258, https://doi.org/10.1016/j.cardiores.2006.05.001.
[21] M. Ott, V. Gogvadze, S. Orrenius, B. Zhivotovsky, Mitochondria, oxidative stress and cell death, Apoptosis 12 (5) (2007) 913–922, https://doi.org/10.1007/s10495-007-0756-2.
[22] S. Gandhi, A.Y. Abramov, Mechanism of oxidative stress in neurodegeneration, Oxid. Med. Cell. Longev. (2012), https://doi.org/10.1155/2012/428010, 2012.
[23] I. Marrocco, F. Altieri, I. Peluso, Measurement and clinical significance of biomarkers of oxidative stress in humans, Oxid. Med. Cell. Longev. 2017 (2017), https://doi.org/10.1155/2017/6501046.
[24] B. Halliwell, M. Whiteman, Measuring reactive species and oxidative damage in vivo and in cell culture: how should you do it and what do the results mean? Br. J. Pharmacol. 142 (2) (2004) 231–255, https://doi.org/10.1038/sj.bjp.0705776.
[25] V. Suresh, J.L. West, 3D culture facilitates VEGF-stimulated endothelial differentiation of adipose-derived stem cells, Ann. Biomed. Eng. 48 (3) (2020) 1034–1044, https://doi.org/10.1007/s10439-019-02297-y.
[26] H. Ardalani, S. Sengupta, V. Harms, V. Vickerman, J.A. Thomson, W.L. Murphy, 3-D culture and endothelial cells improve maturity of human pluripotent stem cell-derived hepatocytes, Acta Biomater. 95 (2019) 371–381, https://doi.org/10.1016/j.actbio.2019.07.047.
[27] B. Andrée, et al., Formation of three-dimensional tubular endothelial cell networks under defined serum-free cell culture conditions in human collagen hydrogels, Sci. Rep. 9 (1) (2019) 1–11, https://doi.org/10.1038/s41598-019-41985-6.
[28] V. van Duinen, S.J. Trietsch, J. Joore, P. Vulto, T. Hankemeier, Microfluidic 3D cell culture: from tools to tissue models, Curr. Opin. Biotechnol. 35 (2015) 118–126, https://doi.org/10.1016/j.copbio.2015.05.002.
[29] Y.B. Arik, et al., Microfluidic organ-on-a-chip model of the outer blood-retinal barrier with clinically relevant read-outs for tissue permeability and vascular structure, Lab Chip 21 (2) (2021) 272–283, https://doi.org/10.1039/d0lc00639d.
[30] H. Somaweera, S.O. Haputhanthri, A. Ibraguimov, D. Pappas, On-chip gradient generation in 256 microfluidic cell cultures: simulation and experimental validation, Analyst 140 (15) (2015) 5029–5038, https://doi.org/10.1039/c5an00481k.
[31] J. Ouyang, R. Li, H. Shi, J. Zhong, X. Shi, Curcumin protects human umbilical vein endothelial cells against H2O2-induced cell injury, Pain Res. Manag. 2019 (2019), https://doi.org/10.1155/2019/3173149.
[32] X. Zhou, et al., Resveratrol regulates mitochondrial reactive oxygen species homeostasis through Sirt3 signaling pathway in human vascular endothelial cells, Cell Death Dis. 5 (12) (2014) 1–13, https://doi.org/10.1038/cddis.2014.530.
[33] X.L. Lin, et al., Inhibition of hydrogen peroxide-induced human umbilical vein endothelial cells aging by allicin depends on sirtuin1 activation, Med. Sci. Mon. 23 (2017) 563–570, https://doi.org/10.12659/MSM.899730.
[34] M. Moussavi, K. Assi, A. Gómez-Muñoz, B. Salh, Curcumin mediates ceramide generation via the de novo pathway in colon cancer cells, Carcinogenesis 27 (8) (2006) 1636–1644, https://doi.org/10.1093/carcin/bgi371.
[35] J.R. Heo, S.M. Kim, K.A. Hwang, J.H. Kang, K.C. Choi, Resveratrol induced reactive oxygen species and endoplasmic reticulum stress-mediated apoptosis, and cell cycle arrest in the A375SM malignant melanoma cell line, Int. J. Mol. Med. 42 (3) (2018) 1427–1435, https://doi.org/10.3892/ijmm.2018.3732.
[36] X. Zhou, et al., Resveratrol attenuates endothelial oxidative injury by inducing autophagy via the activation of transcription factor EB, Nutr. Metab. 16 (1) (2019) 1–12, https://doi.org/10.1186/s12986-019-0371-6.
[37] S. Corda, C. Laplace, E. Vicaut, J. Duranteau, Rapid reactive oxygen species production by mitochondria in endothelial cells exposed to tumor necrosis factor-α is mediated by ceramide, Am. J. Respir. Cell Mol. Biol. 24 (6) (2001) 762–768, https://doi.org/10.1165/ajrcmb.24.6.4228.
[38] V. Van Duinen, et al., 96 perfusable blood vessels to study vascular permeability in vitro, Sci. Rep. 7 (1) (2017) 1–11, https://doi.org/10.1038/s41598-017-14716-y.
[39] S.J. Trietsch, et al., Membrane-free culture and real-time barrier integrity assessment of perfused intestinal epithelium tubes, Nat. Commun. 8 (262) (2017) 1–7, https://doi.org/10.1038/s41467-017-00259-3.
[40] V. van Duinen, D. Zhu, C. Ramakers, A.J. van Zonneveld, P. Vulto, T. Hankemeier, Perfused 3D angiogenic sprouting in a high-throughput in vitro platform, Angiogenesis 22 (1) (2019) 157–165, https://doi.org/10.1007/s10456-018-9647-0.
[41] A. Gomes, E. Fernandes, J.L.F.C. Lima, Fluorescence probes used for detection of reactive oxygen species, J. Biochem. Biophys. Methods 65 (2–3) (2005) 45–80, https://doi.org/10.1016/j.jbbm.2005.10.003.
[42] V. van Duinen, et al., Robust and scalable angiogenesis assay of perfused 3D human ipsc-derived endothelium for anti-angiogenic drug screening, Int. J. Mol. Sci. 21 (13) (2020) 1–9, https://doi.org/10.3390/ijms21134804.
[43] J.A. Royall, H. Ischiropoulos, Evaluation of 2′,7′-dichlorofluorescin and dihydrorhodamine 123 as fluorescent probes for intracellular H2O2 in cultured endothelial cells, Arch. Biochem. Biophys. 302 (2) (1993) 348–355, https://doi.org/10.1006/abbi.1993.1222.
[44] J. Egea, et al., European contribution to the study of ROS: a summary of the findings and prospects for the future from the COST action BM1203 (EU-ROS), Redox Biol. 13 (May) (2017) 94–162, https://doi.org/10.1016/j.redox.2017.05.007.
[45] C.H. Kennedy, D.F. Church, G.W. Winston, W.A. Pryor, Tert-butyl hydroperoxide-induced radical production in rat liver mitochondria, Free Radic. Biol. Med. 12 (5) (1992) 381–387, https://doi.org/10.1016/0891-5849(92)90087-W.
[46] O. Kučera, et al., The effect of tert -butyl hydroperoxide-induced oxidative stress on lean and steatotic rat hepatocytes in vitro, Oxid. Med. Cell. Longev. 2014 (2014), https://doi.org/10.1155/2014/752506.
[47] G. Pharaoh, D. Pulliam, S. Hill, K. Sataranatarajan, H. Van Remmen, Ablation of the mitochondrial complex IV assembly protein Surf1 leads to increased expression of the UPRMT and increased resistance to oxidative stress in primary cultures of fibroblasts, Redox Biol. 8 (2016) 430–438, https://doi.org/10.1016/j.redox.2016.05.001.
[48] W. Zhao, H. Feng, W. Sun, K. Liu, J.J. Lu, X. Chen, Tert-butyl hydroperoxide (t-BHP) induced apoptosis and necroptosis in endothelial cells: roles of NOX4 and mitochondrion, Redox Biol. 11 (2017) 524–534, https://doi.org/10.1016/j.redox.2016.12.036. January.
[49] J. Lin, et al., Gastrodin alleviates oxidative stress-induced apoptosis and cellular dysfunction in human umbilical vein endothelial cells via the nuclear factor-erythroid 2-related factor 2/heme oxygenase-1 pathway and accelerates wound healing in vivo, Front. Pharmacol. 10 (OCT) (2019) 1–12, https://doi.org/10.3389/fphar.2019.01273.
[50] S. Masood, et al., Live cell imaging of oxidative stress in human airway epithelial cells exposed to isoprene hydroxyhydroperoxide, Redox Biol. 51 (2022), 102281, https://doi.org/10.1016/j.redox.2022.102281. February.

[51] D. Jia, et al., Salvianic acid A sodium protects HUVEC cells against tert-butyl hydroperoxide induced oxidative injury via mitochondria-dependent pathway, Chem. Biol. Interact. 279 (October 2017) 234–242, https://doi.org/10.1016/j.cbi.2017.10.025, 2018.
[52] K.J. Jang, et al., Reproducing human and cross-species drug toxicities using a Liver-Chip, Sci. Transl. Med. 11 (2019) 517, https://doi.org/10.1126/scitranslmed.aax5516.
[53] Y. Sun, X.F. Yin, Y.Y. Ling, Z.L. Fang, Determination of reactive oxygen species in single human erythrocytes using microfluidic chip electrophoresis, Anal. Bioanal. Chem. 382 (7) (2005) 1472–1476, https://doi.org/10.1007/s00216-005-3352-8.
[54] A. Junaid, et al., Metabolic response of blood vessels to TNFα, Elife 9 (2020) 1–17, https://doi.org/10.7554/eLife.54754.
[55] H.J. Hsieh, C.A. Liu, B. Huang, A.H. Tseng, D.L. Wang, Shear-induced endothelial mechanotransduction: the interplay between reactive oxygen species (ROS) and nitric oxide (NO) and the pathophysiological implications, J. Biomed. Sci. 21 (1) (2014) 1–15, https://doi.org/10.1186/1423-0127-21-3.
[56] P. Vulto, S. Podszun, P. Meyer, C. Hermann, A. Manz, G.A. Urban, Phaseguides: a paradigm shift in microfluidic priming and emptying, Lab Chip 11 (9) (2011) 1596–1602, https://doi.org/10.1039/C0LC00643B.
[57] G.M. Walker, D.J. Beebe, A passive pumping method for microfluidic devices, Lab Chip 2 (3) (2002) 131–134, https://doi.org/10.1039/b204381e.